Supporting Information for

Distinctive sources govern organic aerosol fractions with different degrees of oxygenation in the urban atmosphere

Ruichen Zhou, Qingcai Chen, Jing Chen, Lujie Ren, Yange Deng, Petr Vodička, Dhananjay K.Deshmukh, Kimitaka Kawamura, Pingqing Fu, Michihiro Mochida*

*Corresponding author: mochida.michihiro@g.mbox.nagoya-u.ac.jp

This PDF file includes:

Text S1 to S6

Figures S1 to S14

Tables S1 to S5

SI References

S1. Acronym definitions

WSOM: water-soluble organic matter

WISOM: water-insoluble organic matter

HULIS: humic-like substances

HP-WSOM: high-polarity fraction of water-soluble organic matter

EOM: extracted organic matter

HR-AMS: high-resolution time-of-flight aerosol mass spectrometer

PMF: positive matrix factorization

FFOA: fossil fuel organic aerosol

BBOA: biomass burning organic aerosol

COA: cooking-like organic aerosol

LO-OOA: less oxidized oxygenated organic aerosol

MO-OOA: more oxidized oxygenated organic aerosol

S2. Fractionation of aerosol extracts by solid-phase extraction

An Oasis HLB column was used to separate WSOM into HULIS and HP-WSOM fractions in a one-step method.[1, 2] First, aerosol extract solutions containing WSOM were adjusted to a pH of 2 using 1 M HCl solution (Sigma) and then loaded in an Oasis HLB column (200 mg). Before loading, the HLB column was preactivated by 6 mL of methanol, followed by rinsing 3 times with 6 mL of water to remove residual methanol. After the solution of WSOM was passed through the HLB column, the column was rinsed three times with 0.5 mL of 0.01 M HCl solution. The effluent was regarded as the HP-WSOM fraction because it should contain highly polar components.[1] The HLB column was dried using high-purity N_2, followed by adding 6 mL of methanol to elute adsorbed compounds from the column. This fraction was referred to as HULIS. Ammonia, which was used to increase the efficiency of elution in some previous studies, was not used to avoid possible contamination and reactions. Wu et al.[3] claimed that 6 mL of methanol efficiently eluted adsorbed atmospheric aerosol samples on a 60 mg HLB column without using ammonia based on a recovery test using Suwannee River Fulvic Acid (SRFA). Several other studies were also performed without ammonia.[4, 5]

The recovery of the use of the HLB column in this study was assessed as follows with four samples. WSOM in these samples was divided into two parts, one for the extraction based on SPE and the other for the analysis of WSOM. The fractions from SPE (HULIS and HP-WSOM) and WSOM were quantified using AMS. The recovery of the SPE analysis using the HLB column was then calculated as the sum of HULIS and HP-WSOM divided by WSOM (Table S2). The recovery was from 93% to 103%, indicating that almost all of the adsorbed compounds were eluted from the HLB column by this method.

S3. Analysis of organic functional groups, organic/elemental carbon, and anhydrous sugars

Five to six samples collected in each season (22 samples in total) were also subjected to FT-IR analysis. Each extract solution was mixed with KBr powder (0.2 g) and fully dried with high-purity N_2 gas. Then, the mixture of the extract and KBr was ground in an agate mortar and analyzed using an FT-IR spectrometer (6100, JASCO) with a diffuse reflectance accessory. The sample was scanned from 600 to 4000 cm^{-1} 64 times to obtain diffuse reflectance FT-IR spectra. The spectrum of pure KBr was subtracted to determine the baseline. The units of the spectra were converted into Kubelka-Munk units. Band fitting for the spectra[6, 7] were performed for the quantification of the relative mass concentrations of eight types of functional groups: alkyl (C–H), hydroxyl (C–OH), nonacidic carbonyl (C=O), carboxylic acid (–COOH), aromatic (C–H), alkene (C=C), amine ($C–NH_2$) and organonitrate ($C–ONO_2$) groups. The O/C and OM/OC ratios of HULIS and WISOM were obtained based on the quantification of the functional groups. The details of the quantification can be found elsewhere.[6, 7]

Organic carbon and elemental carbon were analyzed using an OC/EC Carbon Aerosol Analyzer (Sunset Laboratory Inc., USA) with the thermal optical transmittance (TOT) method following the NIOSH protocol. All samples were corrected based on the analysis of blank samples. Three biomass burning tracers, levoglucosan, galactosan, and mannosan, were measured by traditional gas chromatography-mass spectrometry (GC/MS).[8] In brief, a filter was extracted with dichloromethane/methanol (2:1, v/v) under ultrasonication. The extracts were then concentrated, dried under nitrogen gas, and allowed to react with N,O-bis-(trimethylsilyl)trifluoroacetamide (BSTFA) containing 1% trimethylsilyl chloride at 70 ℃ for 3 h. After the reaction, the internal standard solvent of C_{13} n-alkane was added before GC/MS analysis. GC/MS was performed using a Hewlett-Packard system (7890A GC coupled to 5975C MSD) with a splitless injection and a

fused silica capillary column (DB-5MS) with a programmed GC oven temperature. Concentrations of biomass burning tracers were quantified using GC/MS response factors acquired using authentic standards. The concentrations of OC/EC and three biomass burning tracers were previously reported elsewhere.[9, 10]

S4. Quality control of AMS and FT-IR analysis

For the AMS analysis, three blank filters collected before, during and after a series of atmospheric samplings (Table S1) were extracted and analyzed in the same manner as the TSP samples. The AMS spectra of blank samples were similar to those obtained from the nebulized water, and the intensity of the ion signals of total OA corresponded to 14.3%, 11.0%, and 9.6% of those of HP-WSOM, HULIS, and WISOM with the lowest solution concentrations, respectively. Considering that the transmission efficiency of aerosol particles in the aerodynamic lens of the AMS is size dependent, the mass of OA detected by the AMS is not proportional to the amount of nonrefractory nonvolatile compounds in blank and atmospheric aerosol samples. For this reason, we also measured the numerical size distributions of aerosol particles generated by the nebulization of blank and atmospheric sample solutions using a scanning mobility particle sizer (SMPS); the results are presented in Figure S10. If particles nebulized from the atomizer are assumed to be spherical and the density of organics is similar between blank and sample solutions, the particulate mass can be compared from the estimate of particle volume concentrations. In this analysis, the blank samples corresponded in volume to 10.2–18.3% of the solutions with the lowest concentrations of OA fractions. To assess the repeatability of the offline AMS analysis, two filter samples were extracted and analyzed in duplicate, and the relative standard deviation (RSD) was approximated as the mean of the standard deviation values. The RSDs of the AMS-derived concentrations of HP-WSOM, HULIS, and WISOM were 12.7%, 6.1%, and 2.2%, respectively.

The estimated RSDs of the relative intensities of eight fragment groups (C_xH_y, $C_xH_yO_1$, $C_xH_yO_{>1}$, $C_xH_yN_z$, $C_xH_yON_z$, $C_xH_yO_{>1}N_z$, CS, H_yO_q) were in the range of 1.1–18.2% for HP-WSOM, HULIS, and WISOM except for $C_xH_yON_z$ and $C_xH_yO_{>1}N_z$ of HP-WSOM with a high RSD (37.5–55.5%), which was possibly caused by low concentrations of $C_xH_yON_z$ and $C_xH_yO_{>1}N_z$ (< 1%) in HP-WSOM. In the quantification of sample solutions, two solutions of each fraction were quantified in duplicate, and their RSDs obtained in the manner described for the AMS analysis were in the range of 1–20%. Note that the solutions of some OA fractions were reanalyzed, among which two HP-WSOM showed large decreases in the concentration values (>30%). Because the carbon concentrations of EOM from the original concentrations considerably exceeded those of OC from the thermal analysis (by 77% and 26%), the original concentration values of these two samples would be erroneous and were substituted with those from the reanalysis.

The solutions from the two blank filters were also subjected to FT-IR analysis, and the obtained spectra were compared with those from the sample with the lowest atmospheric OC concentration (Figure S11). The intensities of the FT-IR signal of the blank spectra in the K-M unit corresponded to 0.3–14.9% of those of the sample spectra in the wavenumbers of functional group regions (regions are presented in Figure S1). Some sample spectra, which were considered to be influenced by water, were reanalyzed after drying the sample-KBr mixtures.

S5. FT-IR spectra

The FT-IR spectra of HP-WSOM, HULIS, and WISOM are presented in Figure S1 with qualitative and quantitative information on eight typical functional groups. Their seasonal variations are presented in Figure S2.

The HULIS contributions were mainly alkane (43%), nonacid carbonyl (23%), alcohol (15%), and carboxylic acid (12%) groups with an O/C ratio of 0.41. The high proportion of nonacid carbonyl groups implied a contribution from biomass burning.[11] Hydroxyl and carboxylic acid groups showed higher proportions in autumn and winter. Small amounts of alkene (3%) and aromatic (2%) groups also contributed to HULIS.

WISOM was dominated by alkyl groups, which contributed 80% of OM. The proportion was similar to that in the urban air of Nagoya, Japan (77%).[6] The FT-IR-derived high proportion of alkyl groups was similar to that of the fuel combustion profile from PMF analysis.[11] This similarity and the low O/C ratio of WISOM (0.1) suggested that fuel combustion contributed greatly to this fraction. In addition to the alkyl groups, nonacid carbonyl and hydroxyl groups accounted for 9% and 5% of OM, respectively. The relative contributions of alkyl group decreased in autumn and winter, which could result from enhanced biomass burning in autumn and winter in Beijing and the surrounding areas.[12]

The FT-IR spectra of HP-WSOM could be strongly affected by inorganic salts, which hampers the precise quantification of functional groups. However, hydroxyl groups could be clearly identified in the 3600-3400 cm^{-1} region. Organonitrate was quantified from the peak at 1296–1255 cm^{-1}.[13] It was detectable in most WISOM and HULIS samples with small contributions (mean: 1%).

S6. PMF analysis of AMS spectra

PMF analysis of the collected mass spectra was performed using PMF Evaluation Toolkit (PET) v 3.05, following instructions by Ulbrich et al.[14] In total, 135 extracts were obtained from 45 filter samples, and three high-resolution spectra were recorded for each extract in W-mode

using AMS and used as input data. Each spectrum consisted of 380 HR ions. The corresponding error matrix was calculated according to Allen et al.[15] and Ulbrich et al.[14] The calculation was assessed for factor numbers from 1 to 9 with rotational forcing parameter (fpeak) of zero. The 7-factor solution with a slight change of fpeak was finally selected as the optimal solution, as explained below.

The 1- and 2-factor solutions were not used because both the residual and Q/Q_{exp} (14) were large. Although the Q/Q_{exp} value dropped dramatically when the number of factors increased to three, it still poorly reproduced the three OA fractions (HP-WSOM, HULIS, and WISOM). A 4-factor solution (Figure S13a) separated several factors that can be explained in terms of OA sources, namely, fossil fuel OA (FFOA), cooking-like OA (COA), biomass burning OA (BBOA), and oxygenated OA (OOA). Although FFOA and BBOA were similar to those in the 7-factor solution that are finally chosen for the analysis in this study, COA had a high contribution with a high O/C ratio, implying that the OOA factor was not well separated from the COA factor. The large Q/Q_{exp} value and residuals also suggest that 4 factors did not explain the results well. The COA in a 5-factor solution (Figure S13b) only contributed to HULIS and HP-WSOM, not to WISOM, which contradicted the nature of cooking aerosols. In a 6-factor solution (Figure S13c), the time series of FFOA was different from that of its tracer (EC). In addition, COA was split into two factors that contributed to HULIS and WISOM separately; the COA in WISOM showed a distinct decrease in winter, which contradicted the expectation that cooking activity should be constant throughout a year. Hence, the 6-factor solution was not considered optimal.

In 7-factor solution, FFOA, BBOA, and COA were clearly separated and the other 4 factors were OOA factors characterized by high m/z 43 and 44 peaks and high O/C ratios. The solution with fpeak of −0.2 had a slightly lower Q/Q_{exp} (3.73) than the original solution with fpeak of 0

(3.87), while their mass spectra and time series were nearly identical (SI, 7_factor_solutions.xlxs); the former one was chosen as the optimal solution (Figure S5). In the 7-factor solution (with fpeak of −0.2), FFOA, BBOA, and COA were correlated well with their corresponding tracers (Figure S7). LO-OOA was identified from the relatively high intensity signal of m/z 43 and moderately high O/C ratio (0.56). Other three factors showed similar spectral patterns, with distinct high peaks of m/z 44 and high O/C ratios (0.99–1.57). In addition, these three factors shared similar spectra with those reported by Huang et al.[17], who attributed 3 factors to organic-rich secondary sources, inorganic-rich secondary sources, and dust based on the PMF analysis of offline AMS spectra and molecular tracer data. The sources or formation pathways of these three factors were not identified further but combined as a single MO-OOA factor (Figure S6). Solutions with 8 or 9 factors showed more splits of factors; for example, one of the OOA factors was split into two factors with very similar temporal variations. Considering the above results, we chose the 7-factor solution and combined three OOA factors into a single MO-OOA factor. The final derived PMF factors were FFOA, BBOA, COA, LO-OOA, and MO-OOA.

To assess the relationship between the PMF analysis for extracted OA fractions and the PMF analysis for total OA, spectra from three extract fractions for each filter sample were summed into a single spectrum, followed by PMF analysis (PMF-sum). The resulting spectra could be regarded as similar to the OA spectra from online AMS analysis. A 7-factor solution was selected as the optimal solution (Figure S14), and three factors with similar spectra and high oxygenation levels (O/C ratios > 0.99) were again treated as a single MO-OOA factor (Figure S14b). The resulting five factors had spectra similar to those from the PMF analysis applied to the separate OA fractions (PMF-base). The LO-OOA and MO-OOA from PMF-sum showed temporal variations similar to those from PMF-base. Furthermore, COA presented a time series similar to

that from PMF-base with a higher mean concentration (7.7 versus 3.9 μg m^{-3}). However, BBOA showed lower contributions in spring and summer than those from PMF-base, which was inconsistent with the time series of the BBOA molecular tracers (levoglucosan, galactosan, and mannosan). FFOA exhibited high and low contributions in autumn and winter, respectively, which unlike those in PMF-base. Moreover, FFOA from PMF-sum showed a weaker correlation (R = 0.45) with EC than that from PMF-base (R = 0.68). BBOA, FFOA, COA, LO-OOA, and MO-OOA from PMF-sum contributed 10%, 12%, 23%, 11%, and 44% of the total OA, respectively. The contributions of BBOA, LO-OOA, and MO-OOA were comparable to those from PMF-base and several other source apportionment studies in Beijing.[12, 18] COA showed a higher contribution and FFOA a lower contribution than those from PMF-base and other studies.[12, 18] The comparison of the results from PMF-sum and PMF-base suggested that the two methods were somewhat comparable, but PMF-base resulted in more meaningful PMF factors than PMF-sum, especially for COA and FFOA.

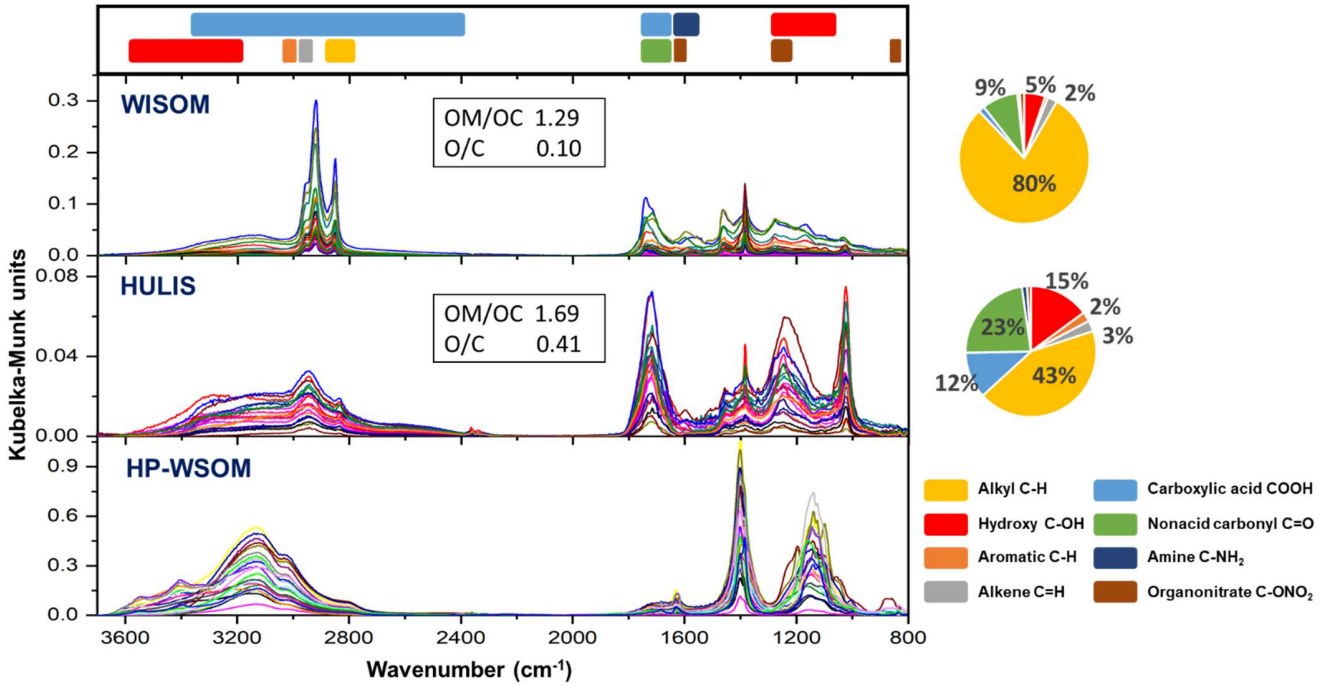

Figure S1. Individual FT-IR spectra of WISOM, HULIS, and HP-WSOM. The pie charts represent the mass fractions of functional groups in WISOM and HULIS. HP-WSOM was considered to be strongly affected by inorganic salts, and therefore its functional groups were not quantified.

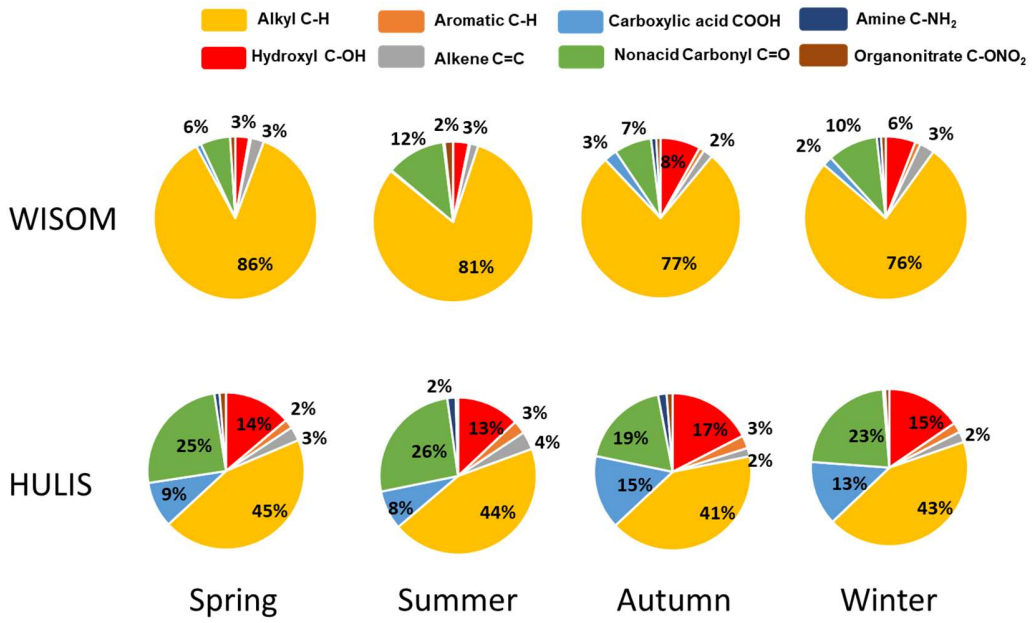

Figure S2. FT-IR-derived mass fractions of functional groups in WISOM and HULIS in different seasons.

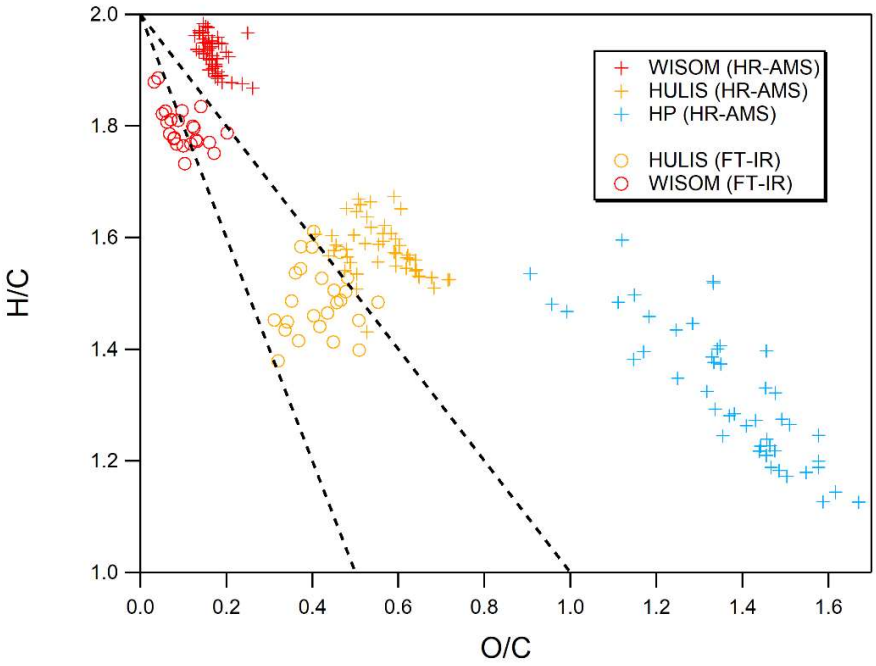

Figure S3. Van Krevelen diagram of HULIS, HP-WSOM, and WISOM from HR-AMS (crosses) and FT-IR (circles) results.

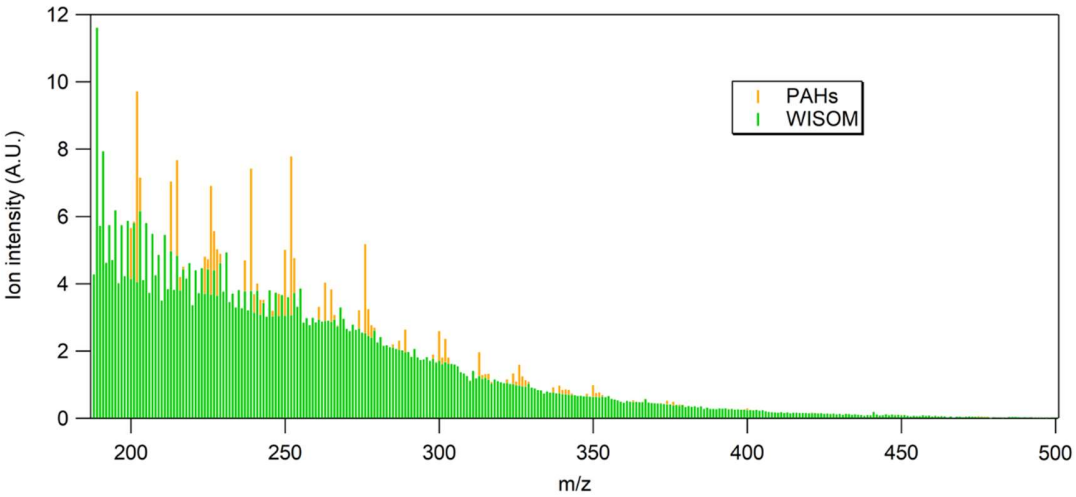

Figure S4. PAH signals (orange bars) assigned in the HR-AMS spectra for WISOM at m/z <500. The green bars represent the ion signals from OA components other than PAHs.

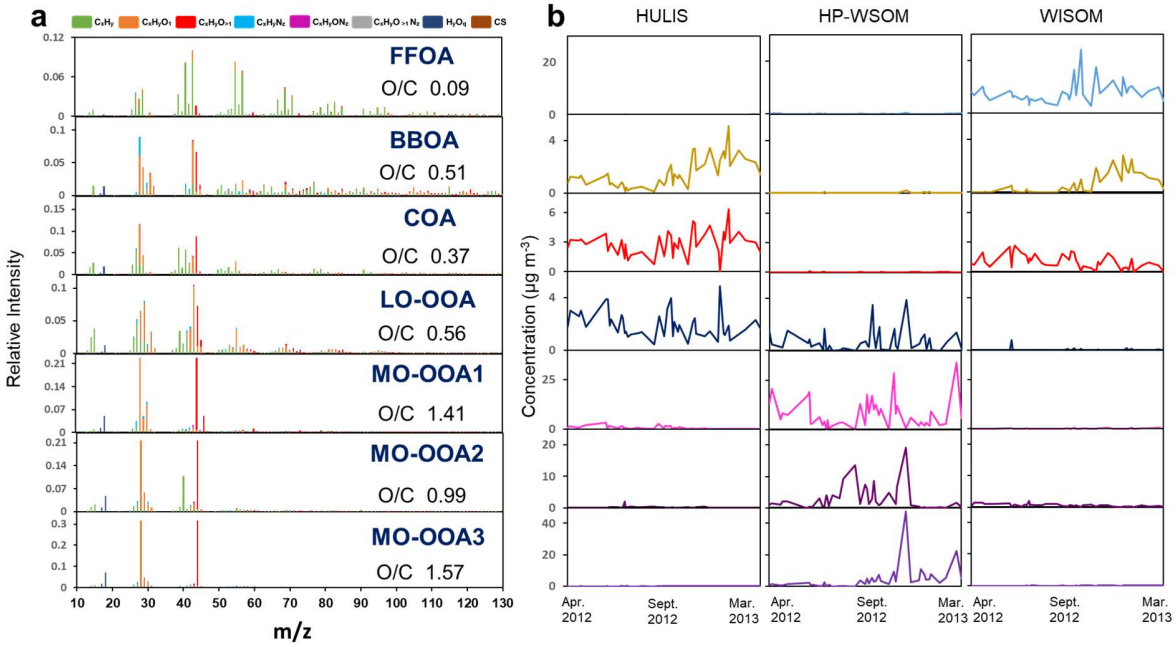

Figure S5. (a) HR-AMS spectra of the 7-factor solution with fpeak of −0.2 from the PMF analysis of HP-WSOM, HULIS, and WISOM, and (b) time series of the seven factors in the three fractions. The factors are fossil fuel OA (FFOA), cooking-like OA (COA), biomass burning OA (BBOA), less oxidized oxygenated OA (LO-OOA), more oxidized oxygenated OA1 (MO-OOA1), MO-OOA2, and MO-OOA3.

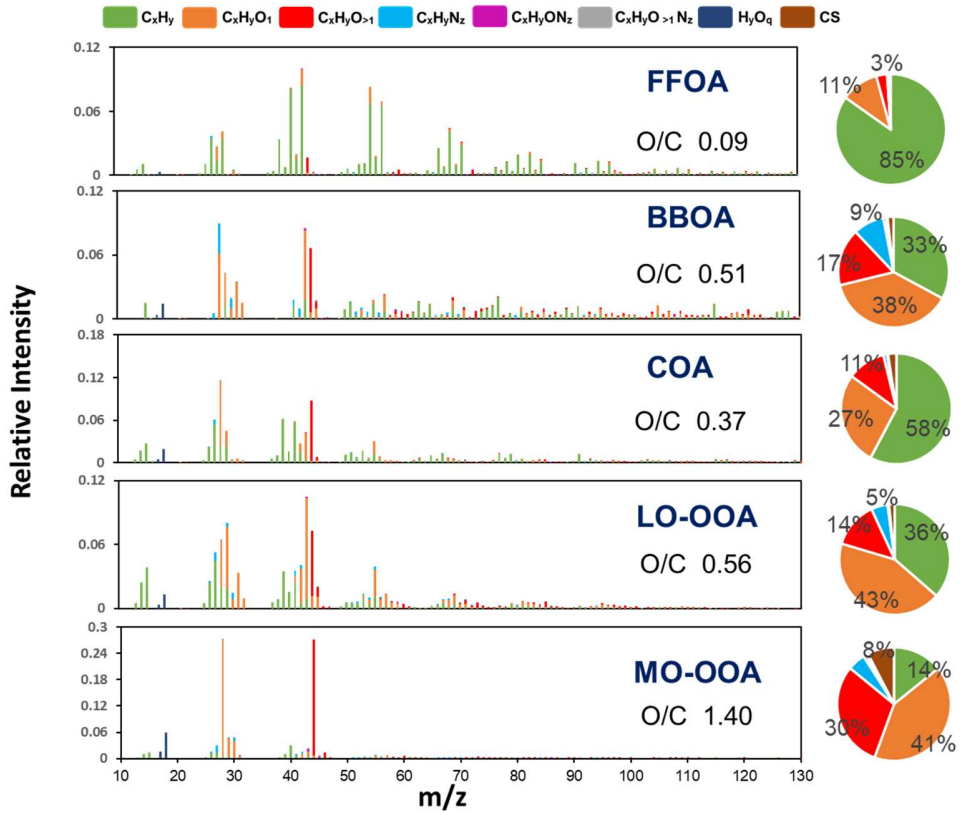

Figure S6. HR-AMS spectra of five PMF factors: fossil fuel OA (FFOA), cooking-like OA (COA), biomass burning OA (BBOA), less oxidized oxygenated OA (LO-OOA), and more oxidized oxygenated OA (MO-OOA). MO-OOA presented here are averages of MO-OOA1, MO-OOA2, and MO-OOA3 factors, with weighting of their atmospheric mass concentrations. The pie charts represent the relative contributions of fragment groups in the factor spectra.

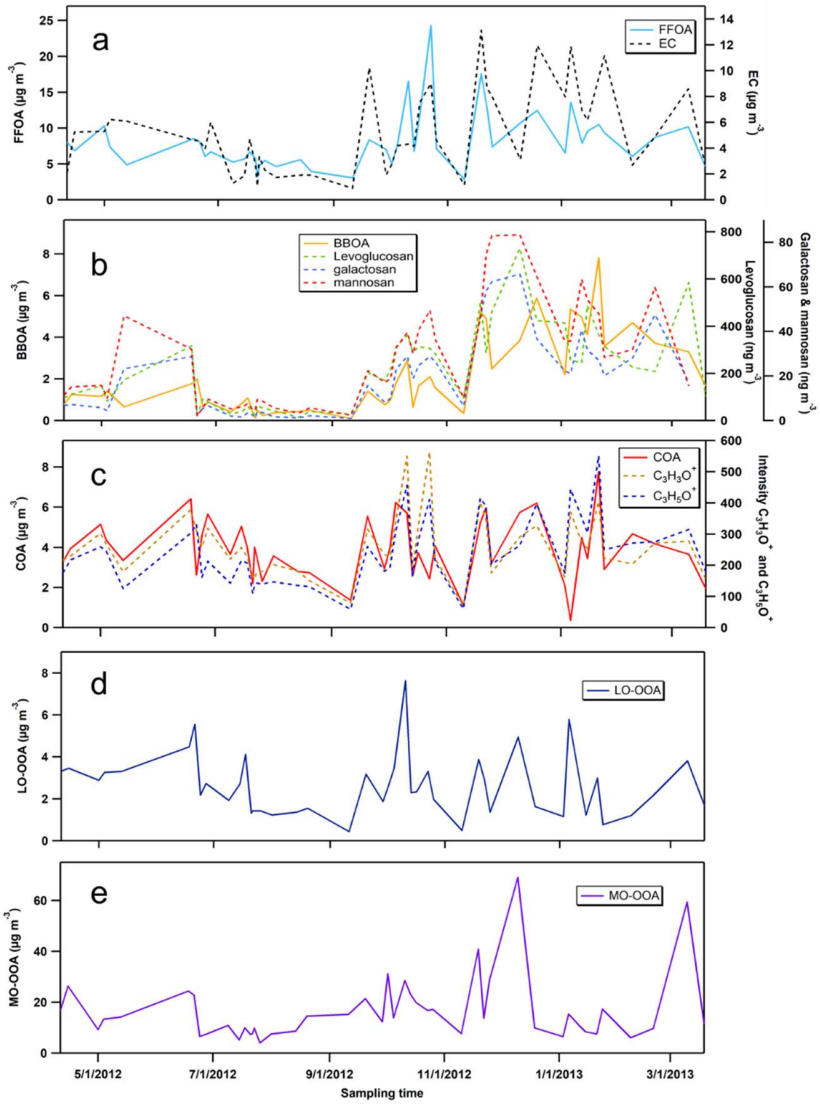

Figure S7. Time series of five factors ((a) FFOA, (b) BBOA, (c) COA, (d) LO-OOA, and (e) MO-OOA) in total OA. The time series of the concentrations of (a) EC, (b) trace fragments of $C_3H_3O^+$ and $C_3H_5O^+$, and (c) levoglucosan, galactosan, and mannosan are also presented.

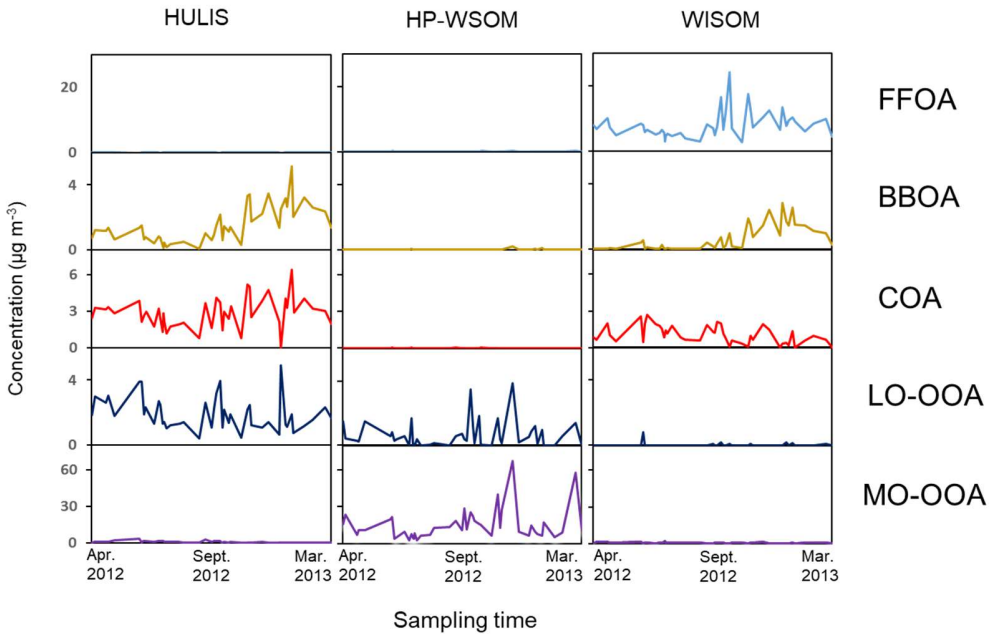

Figure S8. Time series of five factors (FFOA, COA, BBOA, LO-OOA, and MO-OOA) in each fraction (HULIS, HP-WSOM, and WISOM).

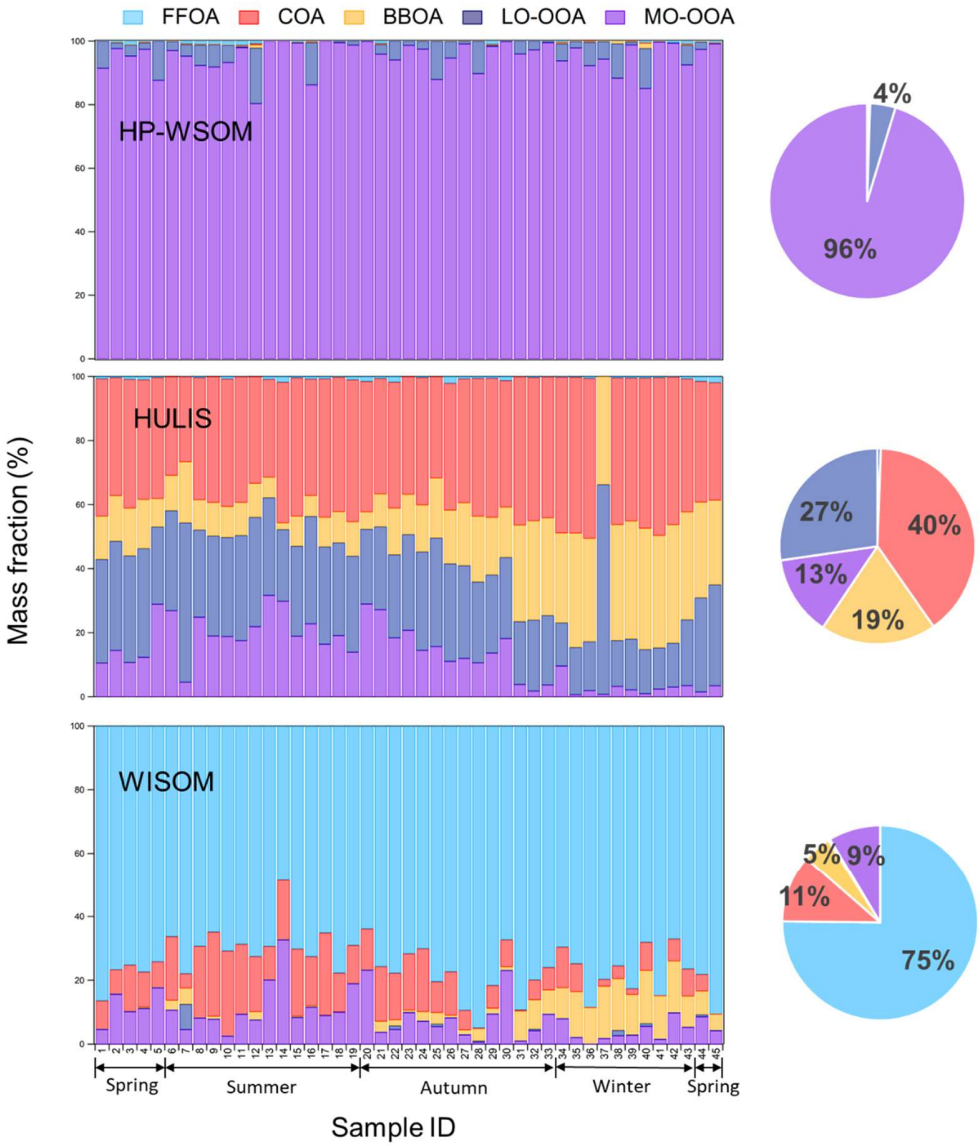

Figure S9. Time series of the mass fractions of five factors (FFOA, COA, BBOA, LO-OOA, MO-OOA) in HULIS, HP-WSOM, and WISOM. The pie charts represent the mean relative contributions of the respective factors.

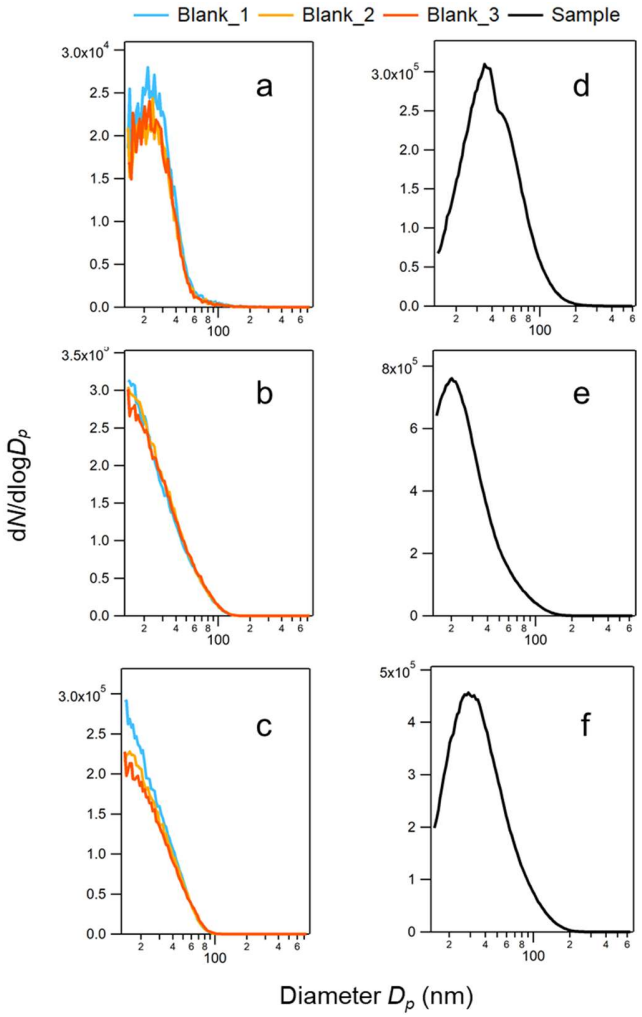

Figure S10. (a, b, c) SMPS-derived number size distributions of aerosols generated from blank solutions prepared to extract (a) HP-WSOM, (b) HULIS, and (c) WISOM and (d, e, f) those generated from atmospheric sample solutions of (d) HP-WSOM, (e) HULIS, and (f) WISOM.

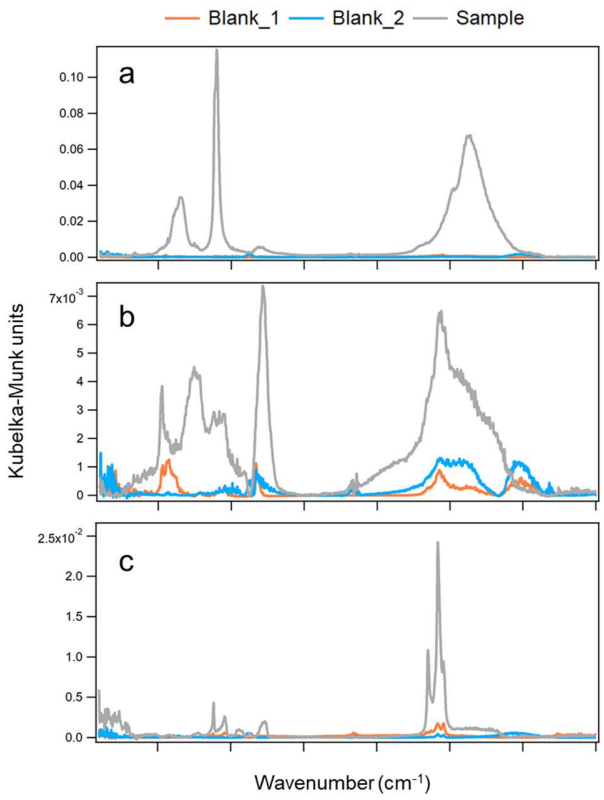

Figure S11. FT-IR spectra of (a) HP-WSOM, (b) HULIS, and (c) WISOM from blank solutions and the sample solutions with the lowest concentrations.

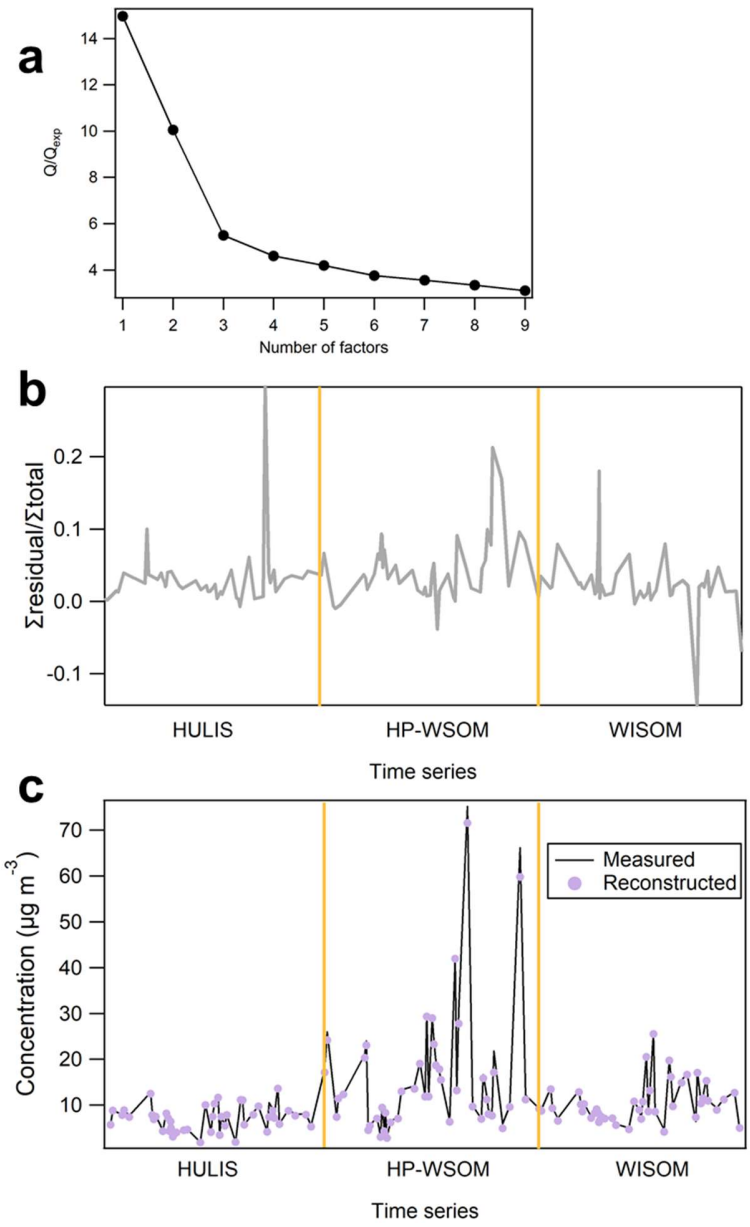

Figure S12. Diagnostics plots of PMF analysis. (a) Q/Q_{exp} values for solutions with different numbers of factors (fpeak = 0), (b) The ratios of residuals to total signal intensities for the 7-factor solution of the PMF analysis, and (c) the reconstructed concentrations from the PMF analysis and the measured concentrations for three OA fractions.

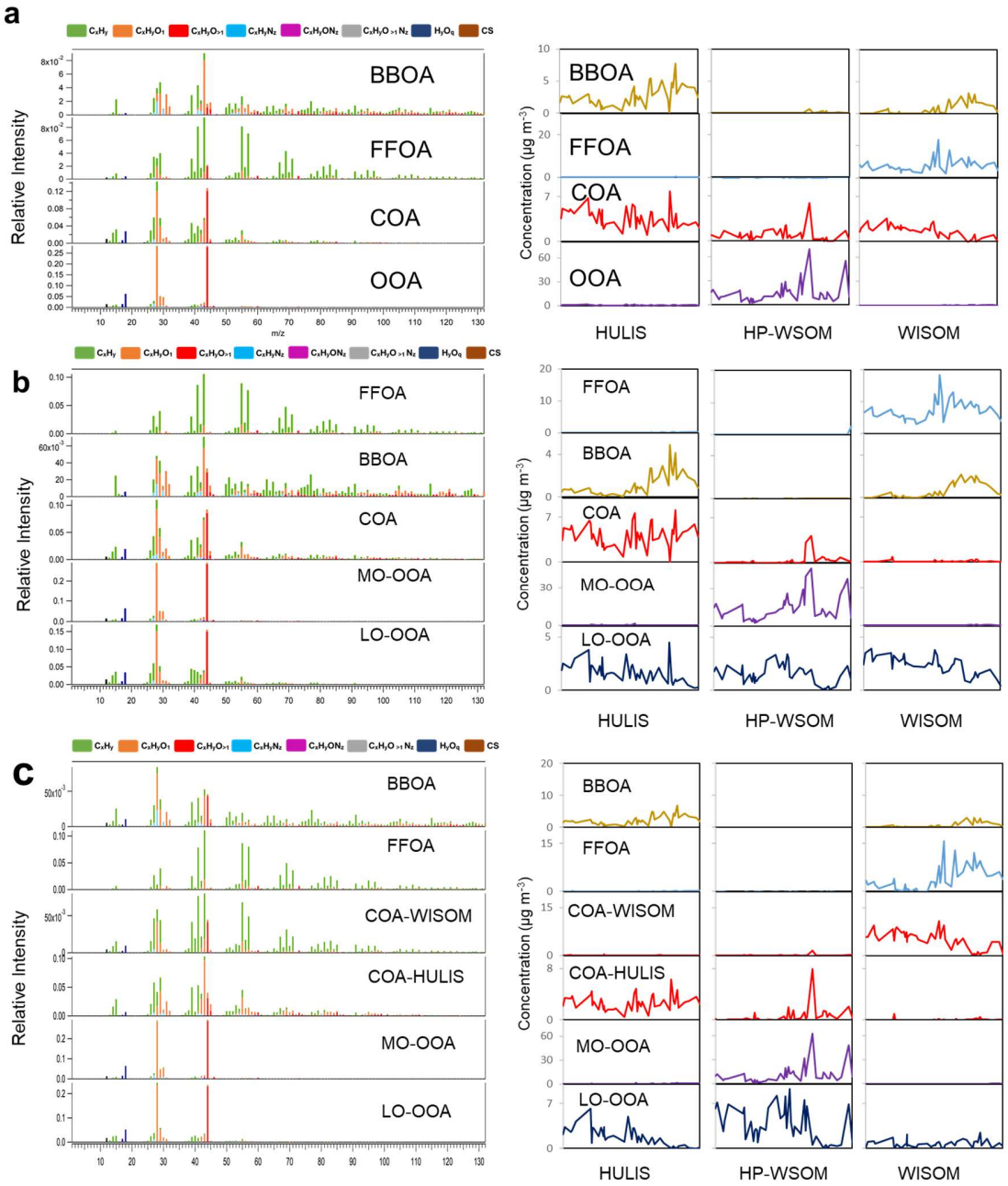

Figure S13. Results from the analysis based on PMF-base method for (a) 4-factor, (b) 5-factor, and (c) 6-factor solutions.

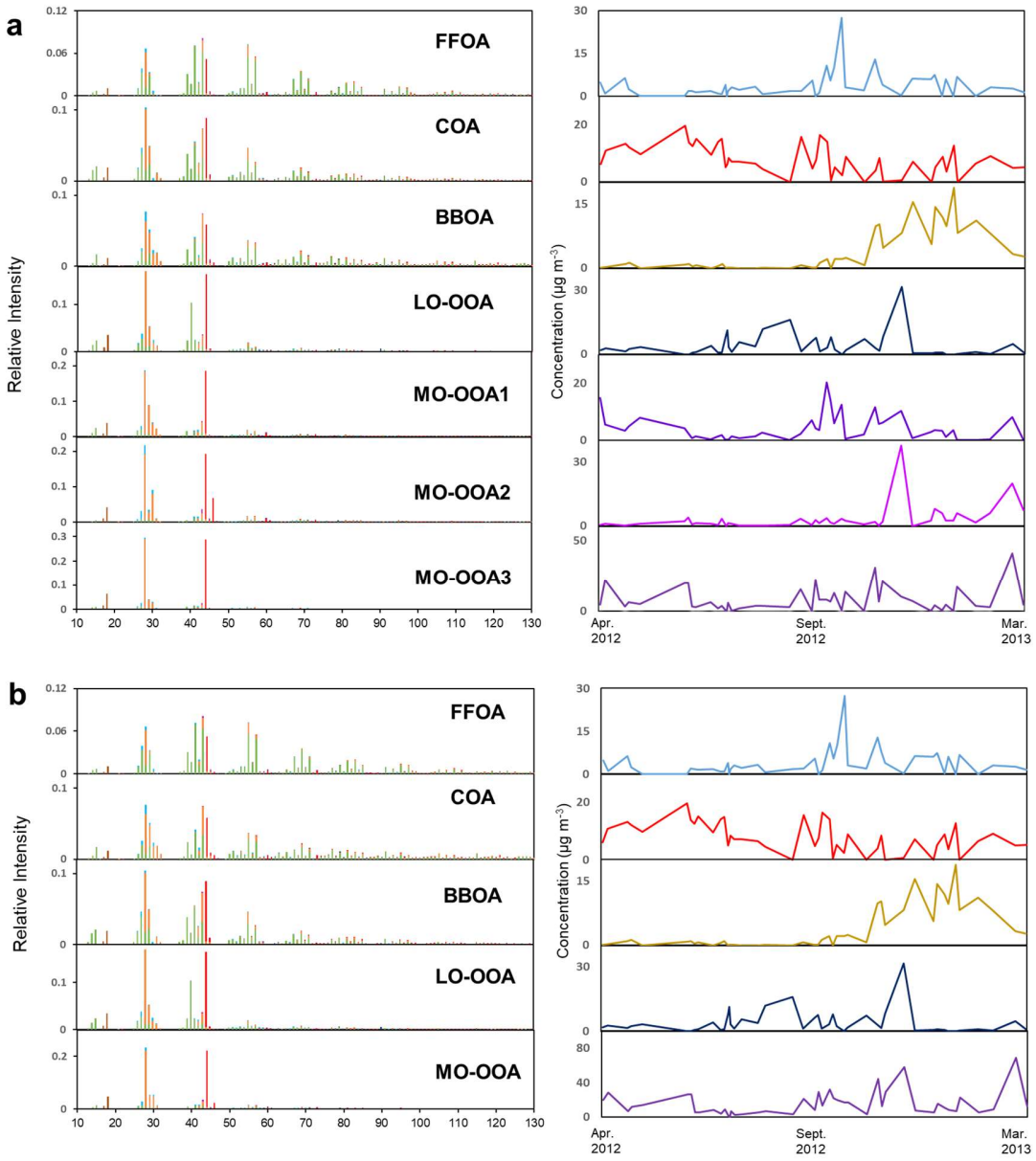

Figure S14. Results from PMF analysis based on the PMF-sum method. (a) HR-AMS spectra and the time series of seven factors. (b) The 5-factor solution derived from the 7-factor solution by combining three similar factors into MO-OOA and the average of the three factors with weighting of their atmospheric mass concentrations.

Table S1. Sample information

Sample ID	Sampling start time	Sampling end time	Duration (h)	Volume (m^3)
1	0910 LT, Apr 11, 2012	0910 LT, Apr 15, 2012	96	5293
2	0913 LT, Apr 15, 2012	0913 LT, Apr 18, 2012	72	4056
3	0910 LT, May 1, 2012	0910 LT, May 4, 2012	72	4085
4	0920 LT, May 4, 2012	0943 LT, May 7, 2012	72	3981
5	0947 LT, May 13, 2012	0947 LT, May 16, 2012	72	4039
6	0837 LT, Jun 18, 2012	0811 LT, Jun 21, 2012	72	3934
7	0825 LT, Jun 21, 2012	0825 LT, Jun 24, 2012	72	3983
8	0857 LT, Jun 24, 2012	0827 LT, Jun 27, 2012	72	3898
9	0837 LT, Jun 27, 2012	0837 LT, Jun 30, 2012	72	4012
10	0904 LT, Jul 9, 2012	0904 LT, Jul 12, 2012	72	3968
11	0810 LT, Jul 15, 2012	0810 LT, Jul 18, 2002	72	3845
12	0821 LT, Jul 18, 2012	0819 LT, Jul 21, 2012	72	3934
13	0826 LT, Jul 21, 2012	1246 LT, Jul 22, 2012	28	1572
14	1255 LT, Jul 22, 2012	1255 LT, Jul 23, 2012	24	1311
15	1325 LT, Jul 23, 2012	0902 LT, Jul 26, 2012	67	3708
16	0907 LT, Jul 26, 2012	0854 LT, Jul 29, 2012	71	3952
17	0853 LT, Aug 1, 2012	0851 LT, Aug 4, 2012	72	3981
18	0938 LT, Aug 14, 2012	0930 LT, Aug 17, 2012	72	3975
19	0909 LT, Aug 20, 2012	0909 LT, Aug 23, 2012	72	3980
20	1003 LT, Sep 11, 2012	0803 LT, Sep 14, 2012	70	3927
21	0851 LT, Sep 20, 2012	0751 LT, Sep 23, 2012	71	3949
22	0933 LT, Sep 29, 2012	0833 LT, Oct 2, 2012	71	4094
23	0902 LT, Oct 2, 2012	0802 LT, Oct 5, 2012	71	3999
24	0850 LT, Oct 5, 2012	0750 LT, Oct 8, 2012	71	4006
25	0913 LT, Oct 11, 2012	0813 LT, Oct 14, 2012	71	4047
26	0908 LT, Oct 14, 2012	0808 LT, Oct 17, 2012	71	4209
27	0906 LT, Oct 17, 2012	0806 LT, Oct 20, 2012	71	4102
28	0912 LT, Oct 23, 2012	0912 LT, Oct 26, 2012	71	4129
29	0850 LT, Oct 26, 2012	0750 LT, Oct 29, 2012	71	4099
30	0913 LT, Nov 10, 2012	0813 LT, Nov 13, 2012	71	4264
31	0813 LT, Nov 19, 2012	0713 LT, Nov 22, 2012	71	4140
32	0805 LT, Nov 22, 2012	0705 LT, Nov 25, 2012	71	4258
33	0809 LT, Nov 25, 2012	0709 LT, Nov 28, 2012	71	3883
34	0840 LT, Dec 10, 2012	0740 LT, Dec 13, 2012	71	3783
35	0900 LT, Dec 19, 2012	0800 LT, Dec 22, 2012	71	3842
36	0840 LT, Jan 3, 2013	0740 LT, Jan 6, 2013	71	4356
37	0842 LT, Jan 6, 2013	0742 LT, Jan 9, 2013	71	4013
38	0910 LT, Jan 12, 2013	0810 LT, Jan 15, 2013	71	4257
39	1012 LT, Jan 15, 2013	0912 LT, Jan 18, 2013	71	4381
40	0940 LT, Jan 21, 2013	0840 LT, Jan 24, 2013	71	3247
41	0857 LT, Jan 24, 2013	0757 LT, Jan 27, 2013	71	4403
42	0855 LT, Feb 8, 2013	1000 LT, Feb 10, 2013	49	3089
43	0815 LT, Feb 20, 2013	0715 LT, Feb 23, 2013	71	4311
44	0757 LT, Mar 10, 2013	0657 LT, Mar 13, 2013	71	4070
45	0810 LT, Mar 19, 2013	0710 LT, Mar 22, 2013	71	4310

Table S2. Recoveries of samples with the use of the SPE technique.

Sample ID	Organic matter (μg m^{-3})				OC-based extraction efficiency (%) [a]	OM-based SPE recovery (%) [b]
	HP-WSOM	HULIS	WISOM	WSOM		
16	3.0	3.2	7.7	6.6	73.8	95.6
26	24.3	3.6	8.9	27.0	94.9	103.4
32	13.2	11.1	16.3	26.1	75.4	93.1
36	7.1	4.2	6.4	12.0	66.3	94.3

a: Calculated by comparing the OC of extracted matter (HP-WSOM + HULIS + WSIOM) and OC from the analysis of filter samples using the OC/EC analyzer.

b: Calculated by comparing the sum of OM of HP-WSOM and HULIS and OM of WSOM.

Table S3. Seasonal concentrations of OM and OC (mean ± SD) of HULIS, HP-WSOM and WISOM, and total OC from thermal OC/EC analysis

	Organic matter (μg m^{-3})			Organic carbon (μg-C m^{-3})			
	HULIS	HP-WSOM	WISOM	HULIS	HP-WSOM	WISOM	Filter
Spring (Mar.–May)	7.6 ± 1.4	21.9 ± 20.4	9.5 ± 3.1	4.0 ± 0.7	6.9 ± 6.2	6.9 ± 2.3	26.7 ± 9.0
Summer (June–Aug.)	6.4 ± 2.5	9.1 ± 6.5	8.5 ± 1.9	3.2 ± 1.2	3.1 ± 2.0	6.1 ± 1.3	16.0 ± 9.4
Autumn (Sept.–Nov.)	7.2 ± 3.5	20.4 ± 9.7	12.2 ± 6.3	3.8 ± 1.8	6.8 ± 3.0	8.9 ± 4.7	23.7 ± 10.4
Winter (Dec.–Feb.)	8.7 ± 2.7	17.5 ± 20.8	12.6 ± 3.6	4.9 ± 1.5	5.9 ± 7.4	8.9 ± 2.5	28.0 ± 11.5
All samples	7.3 ± 2.8	16.5 ± 14.6	10.7 ± 4.5	3.9 ± 1.5	5.5 ± 4.8	7.7 ± 3.3	22.8 ± 10.9

Table S4. The proportions (%) of eight fragment groups from the average HR-AMS spectra for each fraction in different seasons

	C_xH_y	$C_xH_yO_1$	$C_xH_yO_{>1}$	$C_xH_yN_z$	$C_xH_yON_z$	$C_xH_yO_{>1}N_z$	CS	H_yO_q
				HP-WSOM				
Spring	12.6	42.9	30.3	5.7	0.8	0.1	0.4	7.3
Summer	14.6	40.1	29.8	6.9	1.0	0.0	0.4	7.3
Autumn	13.7	41.4	30.2	5.9	0.9	0.0	0.5	7.4
Winter	11.4	41.2	30.4	8.4	1.1	0.1	0.7	6.8
				HULIS				
Spring	40.5	34.9	16.4	4.7	0.6	0.5	0.2	2.2
Summer	37.6	36.2	18.3	3.7	0.5	0.4	0.1	3.3
Autumn	40.5	34.2	16.7	4.8	0.6	0.5	0.2	2.5
Winter	42.0	32.3	17.2	4.6	0.4	1.2	0.4	1.9
				WISOM				
Spring	77.4	14.4	5.7	1.2	0.3	0.2	0.2	0.7
Summer	74.7	16.3	6.4	1.0	0.3	0.1	0.2	0.9
Autumn	77.0	14.6	6.1	1.0	0.3	0.2	0.2	0.6
Winter	71.5	16.8	8.5	1.3	0.3	0.4	0.4	0.9

Table S5. Pearson correlation coefficients between PMF factors and functional groups in HULIS and WISOM.

Functional group	WISOM					HULIS				
	FFOA	COA	BBOA	MO-OOA	LO-OOA	FFOA	COA	BBOA	MO-OOA	LO-OOA
Hydroxyl	0.56	0.33	0.56	0.06	0.11	-0.05	0.47	0.45	-0.04	0.58
Aromatic	0.34	0.01	0.68	-0.11	-0.02	-0.05	0.19	0.16	-0.13	0.34
Alkene	0.60	-0.36	0.17	-0.46	-0.08	-0.27	0.30	0.27	0.15	0.69
Alkyl	0.81	0.14	0.55	-0.04	0.06	-0.03	0.50	0.45	0.00	0.60
Carboxylic acid	0.61	0.25	0.56	0.03	0.01	-0.04	0.46	0.47	0.09	0.54
Nonacid Carbonyl	0.63	0.24	0.77	-0.03	0.08	0.02	0.49	0.36	0.18	0.75
Amine	0.52	0.39	0.59	0.11	0.06	-0.08	0.20	0.05	0.30	0.66
Organonitrate	0.65	0.43	0.55	0.04	0.00	0.53	0.13	0.07	0.02	0.19

SI References

1. Varga, B.; Kiss, G.; Ganszky, I.; Gelencsér, A.; Krivácsy, Z. Isolation of water-soluble organic matter from atmospheric aerosol. *Talanta* **2001,** 55 (3), 561-572.
2. Lin, P.; Yu, J. Z. Generation of reactive oxygen species mediated by humic-like substances in atmospheric aerosols. *Environ. Sci. Technol.* **2011,** 45 (24), 10362-10368.
3. Wu, G.; Wan, X.; Gao, S.; Fu, P.; Yin, Y.; Li, G.; Zhang, G.; Kang, S.; Ram, K.; Cong, Z. Humic-like substances (HULIS) in aerosols of central Tibetan Plateau (Nam Co, 4730 m asl): abundance, light absorption properties, and sources. *Environ. Sci. Technol.* **2018,** 52, 7203–7211.
4. Song, J.; He, L.; Peng, P. a.; Zhao, J.; Ma, S.,Chemical and isotopic composition of humic-like substances (HULIS) in ambient aerosols in Guangzhou, South China. *Aerosol Sci. Tech.* **2012,** 46, 533-546.
5. Wang, Y.; Hu, M.; Lin, P.; Guo, Q.; Wu, Z.; Li, M.; Zeng, L.; Song, Y.; Zeng, L.; Wu, Y.; Guo, S.; Huang, X.; He, L. Molecular characterization of nitrogen-containing organic compounds in humic-like substances emitted from straw residue burning. *Environ. Sci. Technol.* **2017,** 51 (11), 5951-5961.
6. Chen, Q., Ikemori, F., Higo, H., Asakawa, D., Mochida, M. Chemical structural characteristics of HULIS and other fractionated organic matter in urban aerosols: results from mass spectral and FT-IR analysis. *Environ. Sci. Technol.* **2016,** 50 (4), 1721-1730.
7. Takahama, S., Johnson, A., Russell, L. Quantification of carboxylic and carbonyl functional groups in organic aerosol infrared absorbance spectra. *Aerosol Sci. Tech.* **2013,** 47, 310-325.
8. Fu, P.; Kawamura, K.; Miura, K. Molecular characterization of marine organic aerosols collected during a round-the-world cruise. *J. Geophys. Res.* **2011,** 116, D13302.
9. Li, L.; Ren, L.; Ren, H.; Yue, S.; Xie, Q.; Zhao, W.; Kang, M.; Li, J.; Wang, Z.; Sun, Y.; Fu, P. Molecular characterization and seasonal variation in primary and secondary organic aerosols in Beijing, China. *J. Geophys. Res.: Atmos.* **2018,** 123 (21), 12394-12412.
10. Ren, L.; Hu, W.; Hou, J.; Li, L.; Yue, S.; Sun, Y.; Wang, Z.; Li, X.; Pavuluri, C. M.; Hou, S.; Liu, C.-Q.; Kawamura, K.; Ellam, R. M.; Fu, P. Compound-specific stable carbon isotope ratios of terrestrial biomarkers in urban aerosols from Beijing, China." *ACS Earth Space Chem.* **2019,** 3 (9), 1896-1904.
11. Russell, L. M.; Bahadur, R.; Ziemann, P. J. Identifying organic aerosol sources by comparing functional group composition in chamber and atmospheric particles. *Proc. Natl. Acad. Sci. U.S.A.* **2011,** 108 (9), 3516-3521.
12. Sun, Y.; Xu, W.; Zhang, Q.; Jiang, Q.; Canonaco, F.; Prévôt, A. S. H.; Fu, P.; Li, J.; Jayne, J.; Worsnop, D. R.; Wang, Z. Source apportionment of organic aerosol from 2-year highly time-resolved measurements by an aerosol chemical speciation monitor in Beijing, China. *Atmos. Chem. Phys.* **2018,** 18 (12), 8469-8489.
13. Allen, D. T.; Palen, E. J.; Haimov, M. I.; Hering, S. V.; Young, J. R. Fourier transform infrared spectroscopy of aerosol collected in a low pressure impactor (LPI/FTIR): method development and field calibration. *Aerosol Sci. Tech.* **1994,** 21 (4), 325-342.
14. Ulbrich, I.; Canagaratna, M.; Zhang, Q.; Worsnop, D.; Jimenez, J. Interpretation of organic components from positive matrix factorization of aerosol mass spectrometric data. *Atmos. Chem. Phys.* **2009,** 9 (9), 2891-2918.
15. Allan, J. D.; Jimenez, J. L.; Williams, P. I.; Alfarra, M. R.; Bower, K. N.; Jayne, J. T.; Coe, H.; Worsnop, D. R. Quantitative sampling using an Aerodyne aerosol mass spectrometer 1. Techniques of data interpretation and error analysis. *J. Geophys. Res.* **2003,** 108, 4090.
16. Reyes Villegas, E.; Bannan, T. J.; Le Breton, M.; Mehra, A.; Priestley, M.; Percival, C.; Coe, H.; Allan, J. Online chemical characterization of food cooking organic aerosols: implications for source apportionment. *Environ. Sci. Technol.* **2018,** 52 (9), 5308-5318.
17. Huang, R. J.; Zhang, Y.; Bozzetti, C.; Ho, K. F.; Cao, J. J.; Han, Y.; Daellenbach, K. R.; Slowik, J. G.; Platt, S. M.; Canonaco, F.; Zotter, P.; Wolf, R.; Pieber, S. M.; Bruns, E. A.; Crippa, M.;

Ciarelli, G.; Piazzalunga, A.; Schwikowski, M.; Abbaszade, G.; Schnelle-Kreis, J.; Zimmermann, R.; An, Z.; Szidat, S.; Baltensperger, U.; El Haddad, I.; Prevot, A. S. High secondary aerosol contribution to particulate pollution during haze events in China. *Nature* **2014,** 514 (7521), 218-222.

18. Hu, W. W.; Hu, M.; Hu, W.; Jimenez, J. L.; Yuan, B.; Chen, W. T.; Wang, M.; Wu, Y. S.; Chen, C.; Wang, Z. B.; Peng, J. F.; Zeng, L. M.; Shao, M. Chemical composition, sources, and aging process of submicron aerosols in Beijing: contrast between summer and winter. *J. Geophys. Res.: Atmos.* **2016,** 121 (4), 1955-1977.